View metadata, citation and similar papers at core.ac.uk

brought to you by CORE

provided by De Montfort University Open Research Archive

The Significance of Scaling Effects in a Solar Absorber Plate with Micro-Channels

Oyinlola, M.A [*], Shire, G.S.F. and Moss R.W.

School of Engineering, University of Warwick, Gibbet Hill Road, Coventry, UK, CV4 7AL

[*]M.A.Oyinlola@warwick.ac.uk,

Abstract: This paper investigates the significance of some micro scaling effects in micro-channel absorber plates. These plates are to be used in a proposed compact (thin and light-weight) solar thermal flat plate collector (FPC). Forced convection experiments were performed on an instrumented metal plate with micro-channels. Reynolds numbers were in the range 10 – 100 and fluid inlet temperatures ranged from 5 – 40 °C. Scaling effects such as viscous dissipation and entrance effects had insignificant impact on the measured average Nusselt number. However, conjugate heat transfer and measurement uncertainties were significant. Conjugate heat transfer was found to reduce the Nusselt number which agrees with the literature, this also resulted in a Peclet number dependent Nusselt number. The local Nusselt number was observed to vary axially despite satisfying the criteria for neglecting entrance effects; this variation increased with the Graetz number. It was observed that the position of the thermocouples can result in an under-estimation of the Nusselt number. The results are beneficial for the design and operation of micro-channel absorber plates.

Keywords: Microchannel; Scaling effects; Absorber plate; Solar collector; Laminar flow; Conjugate heat transfer

Nomenclature

a	Channel depth (m)
b	Channel width (m)
Br	Brinkman number (-)
c_p	Specific heat capacity (J/kg K)
C	constant
D_h	Hydraulic diameter (m)
F'	Collector Efficiency factor
f	Friction factor (-)
Gz	Graetz Number (-)
h	Heat transfer coefficient (W/m^2 K)
k_p	Thermal conductivity of metal (W/m K)
k_f	Thermal conductivity of fluid (W/m K)
L	Length of channel (m)
L_t	Thermal entry length (m)
L_y	Plate width (m)
$\dot{m}$	Mass flow rate (kg/s)
N_c	Number of channels in plate (-)
Nu	Nusselt number (-)
Pe	Peclet number (-)
Pr	Prandtl number (-)
p	Channel pitch (m)
Q	Heat supplied (W)
q	Heat flux from channel walls (W/m^2)
q_L	Heat flux per unit length (W/m)
Re	Reynolds number (-)
S_c	Total surface area of channels (m^2)
T_f	Average fluid temperature (K)
T_{in}	Fluid temperature at inlet (K)
T_{out}	Fluid temperature at outlet (K)
T_p	Average plate temperature (K)
v_m	Mean fluid velocity (m/s)
ΔT_{pf}	Difference of plate & fluid Temperature (K)
x	Position in flow direction (m)
δ	Plate thickness (m)
ρ	Density (kg/m^3)
μ	Dynamic Viscosity (Pa.s)
ν	Kinematic viscosity (m^2/s)
Δp	Pressure Drop (Pa)
ω	Uncertainty (-)

1. Introduction

Buildings account for the bulk of the energy demand; according to the United Nations Environment Programme (UNEP) *"Buildings use about 40% of global energy ... Yet, buildings also offer the greatest potential for achieving significant GHG emission reductions, at least cost, in developed and developing countries"* [1]. Solar Thermal Flat Plate Collectors (FPCs) are often used as an environmentally friendly alternative to fossil fuel, in meeting the growing thermal energy demand in buildings. The large size of these systems poses a challenge for aesthetically incorporating them in buildings. A viable alternative to the conventional FPC is a Compact (thin and light-weight) Flat Plate Collector (CFPC) [2]. In this collector design, the absorber plate will have micro-channels that replace the conventional arrangement of tubes bonded to a metal sheet. Celata's [3] definition of a microchannel as a channel whose hydraulic diameter lies between 1μm and 1 mm is adopted in this study. In addition to achieving the compact size, this design offers the advantage of enhanced convective heat transfer (based on the premise that the heat transfer coefficient is inversely proportional to the channel's hydraulic diameter), high fin efficiency, uniform temperature distribution in the transverse direction and eliminates the bond resistance between the tubes and absorber sheet in conventional FPC design.

Several scholars have published various approaches to building integration of solar systems [4-7] as well as studies dedicated to optimising absorber plates [8-11], however, there is limited work in the literature on the application of micro-channels to solar systems. Some of the few researchers who have published work in this area include Khamis Mansour [12]; who looked at flat plate rectangular channelled absorber plate, Sharma and Diaz [13] who investigated its application in evacuated tube collector and Deng, et al. [14] who studied a novel FPC with micro-channel heat pipe array.

The theory and correlations of heat transfer and fluid flow in conventional sized rectangular channels are well established; constant Nusselt number in the range 0.457 – 8.235, with the exact value depending on the wall boundary conditions, are expected for fully developed laminar flow [15, 16]. Similarly in terms of friction factor, constant Poiseuille numbers in the range 56.92 – 96.00 are expected for rectangular channels with aspect ratios ranging from 0 – 1. Tuckerman and Pease [17] pioneered the study of heat transfer in microchannels in 1981. Inconsistent results have been published from the extensive study in this field; some studies have found the average Nusselt number to be Reynolds number dependent in the laminar regime [18-20], some recorded lower Nusselt numbers [21-23] while some recorded higher Nusselt numbers [24-27]. Reviews on experimental and numerical studies of heat transfer in micro-channels published by Morini [28], Hetsroni, et al. [29], Rosa, et al. [30] and Sobhan and Garimella [31] confirm the very large scatter in published results and attribute this to "scaling effects". These effects arise from neglecting phenomena which are insignificant in conventional sized channels but become significant as a result of the high channel wall surface to fluid volume ratio in microchannel flow. Examples of these scaling effects include surface roughness [22], entrance and exit effects [27, 32], conjugate heat transfer [23, 33], thermal boundary conditions [34], viscous dissipation [35], electric double layer [36] and increased measurement uncertainties [37]. This paper experimentally studies the significance of some of these "scaling effects" on the performance of the absorber plates.

The significance of these scaling effects can be influenced by the design and application; also, the overall performance can be improved or depreciated, depending on the dominant scaling effects. This suggests that the performance of micro-channel heat sinks should be tested for the particular application. The extensive study on micro-channels has been largely in the context of cooling electronic components. The peculiarities of micro-channel heat transfer application in solar collectors include low Reynolds numbers as well as the low heat flux densities. Most of the previous work done have been conducted for higher flow rates (typically Re>100) and higher heat fluxes (typically q>10,000 W/m^2). This study focuses on flows with Re<100 and q<1000 W/m^2. Also, the flow length in solar collectors will be longer than heat sinks for cooling electronic components. Therefore, scaling effects which are length dependent, such as entrance effects and conjugate heat transfer are likely to differ.

2. Theory

The collector efficiency factor F' is a parameter often used to characterise flat plate collectors. F' represents the ratio of the useful energy gain to the useful gain that would result if the collector absorbing surface had been at the local fluid temperature [38]. Therefore, the convective heat transfer coefficient, h, which determines the temperature difference between the absorber plate and the fluid, is a good parameter for characterising the thermal performance of the plates; the higher the heat transfer coefficient, the lower the temperature difference between plate and fluid, the better the thermal performance of the plate.

Hydraulic performance is one characteristic that will influence plate design. If the energy output is to be maximised, the least possible power must be expended on pumping the fluid. The friction factor, equation(19), which is often used to characterise the hydraulic performance of fluid flow through ducts will be used in this study.

In this paper, the impact of the various scaling effects on the dimensionless heat transfer coefficient, the Nusselt number and the friction factor, will be examined. The scaling effects relevant to this study are discussed below. Others like electric double layer, mixed boundary condition, and rarefaction are insignificant in this study because of the working fluid and low flow velocity.

2.1 Viscous dissipation

Although internal generation of heat is usually neglected in macroscopic flows through channels, at very small hydraulic diameters viscous forces can generate significant internal heat, which can in turn influence the heat transfer [30]. Koo and Kleinstreuer [39] noted that viscous dissipation can be significant in rectangular channels even for low Reynolds numbers. Others who have highlighted the significance of viscous dissipation include Tunc and Bayazitoglu [40], Toh, et al. [41], Morini [28], Herwig and Mahulikar [42], Jeong and Jeong [43] and Chen [44].

The Brinkman number, defined in equations (1)&(2), which is the ratio between the viscous heating rate and the fluid – channel walls average heat transfer rate, is usually employed to evaluate the significance of viscous heating [30]. Equation (3) has been proposed as the criterion for accounting for the effects of viscous heating [28, 30].

For constant wall het flux,

$$Br = \frac{\mu v_m^{\ 2}}{q_L} \tag{1}$$

For constant wall temperature,

$$Br = \frac{\mu v_m^{\ 2}}{k_f \Delta T_{pf}} \tag{2}$$

$$Br < \frac{\xi_{\lim} D_h^{\ 2}}{2(ab)\, fRe} \tag{3}$$

Where ξ_{lim} is the maximum allowable ratio between the temperature rise due to viscous dissipation and the temperature rise due to supplied heat flux at the wall (for example, ξ_{lim}=5%) [30].

2.2 Entrance effects

One of the common scaling effects cited by researchers is entrance effects [27, 45]. Constant local Nusselt numbers are expected for fully developed flow, however, entrance effects can yield a significant variation in predicted and measured average Nusselt number. The Graetz number, *Gz*, defined in equation (4), is used as the criterion for neglecting entrance effects.

$$Gz = \frac{RePrD_h}{L} \tag{4}$$

The entrance effects on the average Nusselt number can be neglected if the inequality in equation (5) is satisfied [28, 30]

$$Gz < 10 \tag{5}$$

2.3 Conjugate heat transfer

Conjugate heat transfer is another scaling effect often cited as having significant influence on the heat transfer in micro-channels [23, 33, 46]. This arises because the hydraulic diameter and the wall thickness of the channels are usually of the same order of magnitude. It therefore becomes necessary to account for the axial thermal conduction in the channel walls, in addition to the forced convective heat transfer. The dimensionless axial conduction number, *M,* defined in equation (6), which can be seen as the ratio of axial thermal conduction to convective heat transfer, can be used to characterise effects of conjugate heat transfer in microchannels [33].

$$M = \frac{k_p}{k_f} \frac{A_{cp}}{A_f} \frac{1}{RePr} \tag{6}$$

Where A_{cp} is the cross sectional area of the solid walls of the channel and A_f is the wetted surface area. The axial thermal conduction in the channel walls can be neglected if the inequality in equation (7) is satisfied [30, 33]

$$M < 0.01 \tag{7}$$

2.4 Experimental Uncertainties

Several studies have cited measurement uncertainties as another possible explanation of the discrepancies between experimental and theoretical results [3, 37, 47]. Some of these uncertainties include channel diameter variation axially, accurately measuring fluid and

channel wall temperatures and assuming similar conditions in all channels. Gamrat, et al. [23] observed that the position of the thermocouples away from the liquid/solid interface can yield as much as 40% uncertainty in the estimated Nusselt number.

3. Experimental Apparatus

3.1 Description of the experimental system

A setup representative of the proposed system was designed for experimental investigation. Figure 1a shows a flow schematic of the experimental facility; a temperature controlled circulating bath supplied the heat transfer fluid, Tyfocor® LS, (a propylene glycol-based heat transfer fluid for solar collectors) at constant flow rate and temperature to a micro-channel test rig. Instruments to measure the temperature at different points, the pressure drop across the test rig and the mass flow rate were embedded at appropriate locations in the loop. A picture of the experimental setup is shown in Figure 1b.

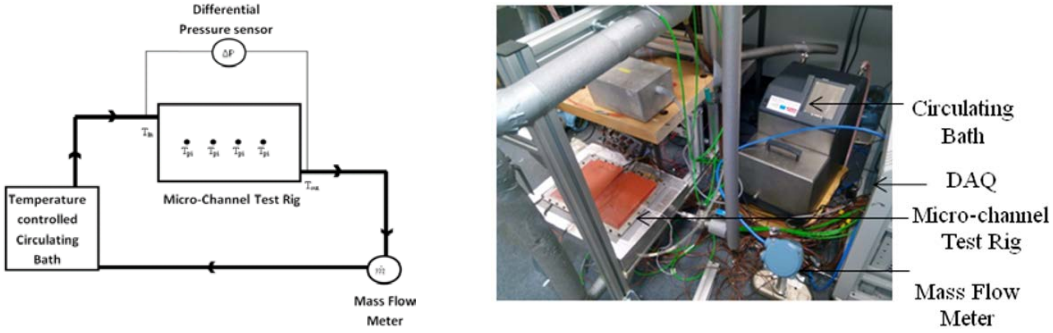

Figure 1: (a) Flow Schematic (b) Experimental apparatus

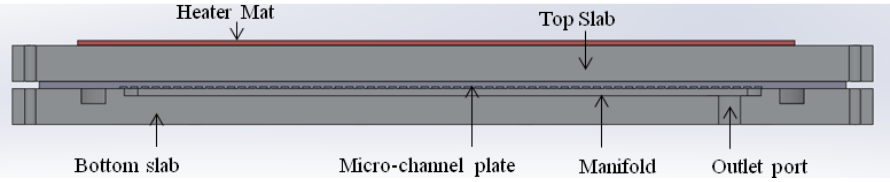

Figure 2: Cross section of test rig

The main component of the experimental setup was the micro-channel test rig which simulated the flat plate collector. It was made up of two 340 × 240 × 10 mm aluminium slabs – a "top" and "bottom" piece, with a thinner (3 mm) channel plate sandwiched between them, as shown in Figure 2. This arrangement allowed a variety of relatively simple channel plates to be tested without each needing its own inlet and outlet connections. Incident solar radiation was simulated with a self-adhesive heater mat, capable of supplying up to 1200 W/m^2, mounted on the top slab. All the data in this paper were obtained with a heater power of about 70W, equivalent to 950 W/m^2. The uniformity of the heat flux imposed by the heater mat was validated in two ways; firstly, an infrared camera was used to check the temperature profile on the resistance heater – a maximum variation of less than 0.25 °C was observed. Secondly, the transient temperature profile of the micro-channel plate was examined when the heater mat was turned on with no flow through the channels. A uniform temperature profile was observed on the plate, which signifies a uniform heat flux from the mat. The rig was insulated with a box

constructed from Polyisocyanurate foam. The channels and manifolds were designed as a Z type heterogeneous ladder with two scale resistance; from the model presented by Tondeur, et al. [48], the mal-distribution in the channels is expected to be less than 20%.

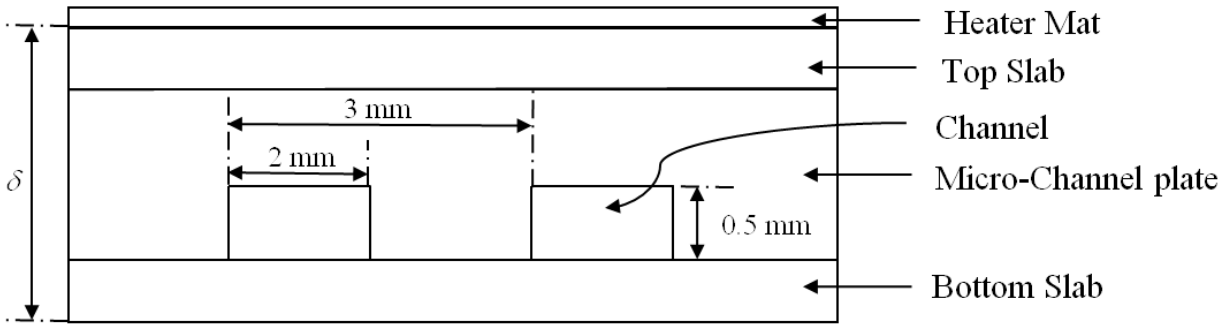

Figure 3: Schematic of Test Rig

A schematic of the test rig is shown in Figure 3 and a picture of the absorber plate can be seen in Figure 4a. The plate had sixty micro-channels, 0.5 mm × 2 mm × 270 mm long and spaced 1 mm apart (3 mm pitch). Temperatures of the plate at different points (T_{pi}), fluid at inlet (T_{in}) and fluid at outlet (T_{out}) were measured using Type T thermocouples. Several thermocouples were fixed on the absorber plate using fibre-glass thermal attachment pads, as shown in Figure 4b. Thermocouples were placed inside the inlet and outlet ports after elbow fittings (to promote fluid mixing) for accurate readings of bulk fluid temperature. All pipes and fittings were properly insulated to minimise heat loss to the ambient. The flow rate ($\dot{m}$) and pressure drop (Δp) were measured using a Coriolis mass flow meter and a differential pressure sensor respectively. All the measured quantities were logged with a 16-bit National Instruments data acquisition system via Labview. Thermocouples were connected through a SCXI-1102 thermocouple interface board. Signals were sampled at 2 Hz; signal quality was studied using an oscilloscope to ensure they were clean and free from interference. Post steady state data were used for analyses. The criterion for steady state was defined by $\frac{dT}{dt} < 2.5 \times 10^{-5}$ °C/s; this was reached after approximately 10–15 minutes at a constant flow rate. The enthalpy change of the fluid was used to calculate the heat flux. A sample of the fluid inlet temperatures and flow rates used for the experiment are shown in Table 1.

Figure 4: (a) Inner face of Test Rig (b) Thermocouple arrangement on plate

Table 1: Experimental run using Tyfocor through 0.5 mm × 2 mm × 270 mm channels

Run	T_{in} (°C)	$\dot{m}$ (g/s)	*Re*	ω_{Re}	*Nu*	ω_{Nu}	L_t/L(%)	*f*	ω_f
1	5.9	12.3	15.9	1.4	0.97	0.11	21.3	0.43	0.05
2	5.9	11.1	14.5	1.3	1.03	0.12	19.2	0.50	0.06
3	6.1	9.2	12.2	1.1	0.95	0.11	15.9	0.69	0.09
4	6.3	7.2	9.9	0.9	0.86	0.10	12.5	0.99	0.12
5	6.5	5.4	7.7	0.7	0.89	0.11	9.3	1.48	0.19
6	7.0	3.6	5.6	0.5	0.78	0.09	6.2	2.65	0.35
7	7.7	2.1	3.6	0.3	0.54	0.05	3.6	5.88	0.84
8	20.4	18.0	47.6	4.2	0.86	0.10	31.1	0.19	0.02
9	20.3	15.3	40.6	3.6	0.87	0.10	26.5	0.20	0.03
10	20.3	12.7	33.8	3.0	0.86	0.10	22.0	0.26	0.03
11	20.3	10.2	27.3	2.4	0.89	0.10	17.6	0.34	0.04
12	20.3	8.0	21.6	1.9	0.85	0.10	13.8	0.47	0.06
13	20.4	5.7	15.6	1.4	0.77	0.08	9.8	0.66	0.08
14	20.5	3.5	9.9	0.9	0.62	0.06	6.0	1.23	0.16
15	39.9	21.4	115.0	10.3	0.63	0.07	36.4	0.11	0.01
16	39.9	18.6	100.0	9.0	0.65	0.07	31.6	0.12	0.02
17	39.9	15.9	85.7	7.7	0.66	0.07	27.1	0.14	0.02
18	39.9	13.2	71.3	6.4	0.67	0.08	22.5	0.17	0.02
19	39.8	10.4	56.3	5.1	0.66	0.07	17.7	0.21	0.03
20	39.7	7.6	41.3	3.7	0.62	0.07	12.9	0.29	0.04
21	39.5	4.9	26.9	2.5	0.55	0.06	8.3	0.44	0.06

3.2 Data Reduction

Each test was run for 15 minutes to reach steady state and 200 data points were then captured. The parameters presented in Table 2 were calculated using the average of the captured data.

3.3 Uncertainty

The Data Acquisition system has a function for calibrating all channels. This procedure compensates for the inaccuracies in the whole measurement system. The thermocouples were bonded together, put in the bath and calibrated at a number of temperatures to match bath temperature readout. The sample standard deviation, for all thermocouples, was typically 0.016 °C. Voltages from the mass flow meter were calibrated to match its display readout while the differential pressure sensor was calibrated to match a hand held manometer. The mass flow meter was also checked by timing flow into a measuring cylinder.

After calibration, steady state measurements were recorded for about 15 minutes. The standard deviation observed in each parameter was taken as the instrument's uncertainty. Uncertainties in geometric parameters were estimated using high precision measuring instruments as well as manufacturers' specifications. The deviations were used to estimate the uncertainties in the calculated values, assuming that the deviations in each term were uncorrelated. For example, equation (8) [49] was used to estimate the uncertainty in the heat transfer coefficient. The uncertainties in some of the measured parameters are shown in Table 1. Further details can be found in [2].

$$\omega_h = h\left[\left(\frac{\omega_Q}{Q}\right)^2 + \left(\frac{\omega_{S_c}}{S_c}\right)^2 + \left(\frac{\omega_{\Delta T_{pf}}}{\Delta T_{pf}}\right)^2\right]^{1/2} \tag{8}$$

Table 2: Details of data reduction

Parameter	Relation	Equation Number
Mean plate temperature	$T_p = \frac{\sum_{i=1}^{n} T_{pi}}{n}$	(9)
Mean fluid temperature	$T_f = \frac{T_{in} + T_{out}}{2}$	(10)
Total surface area of channels	$S_c = 2N_c L(a+b)$	(11)
Heat transferred to fluid	$Q = \dot{m} C_p \left(T_{out} - T_{in}\right)$	(12)
Heat transfer coefficient	$h = \frac{Q}{S_c \left(T_p - T_f\right)}$	(13)
Plate-fluid temperature difference	$\Delta T_{pf} = \left(T_p - T_f\right)$	(14)
Heat flux density	$q = \frac{Q}{S_c} = h\Delta T_{pf}$	(15)
Reynolds number	$Re = \left(\frac{\dot{m}}{abN_c}\right)\frac{D_h}{\mu}$	(16)
Prandtl number	$Pr = \frac{c_p \mu}{k_f}$	(17)
Peclet number	$Pe = RePr$	(18)
Friction factor	$f = \Delta p \frac{D_h}{L} \frac{1}{\frac{1}{2\rho}\left(\frac{\dot{m}}{N_c ab}\right)^2}$	(19)
Nusselt number	$Nu = \frac{hD_h}{k_f}$	(20)
Thermal entry length	$L_t = 0.05 RePrD_h$	(21)
Hydraulic entry length	$L_h = 0.05 ReD_h$	(22)
Axial conduction number	$M = \frac{k_p}{k_f}\frac{D_h}{L}\left(\frac{\delta L_y}{\delta L_y - N_c ab} - 1\right)\frac{1}{RePr}$	(23)
Brinkman number	$Br = \frac{\mu\left(\frac{\dot{m}}{N_c ab}\right)^2}{q_L}$	(24)

4. Results and Discussion

4.1 Results

Experiments were run at three different inlet fluid temperatures (5°C, 20°C and 40°C). For each fluid temperature, seven (7) different mass flow rates were used.

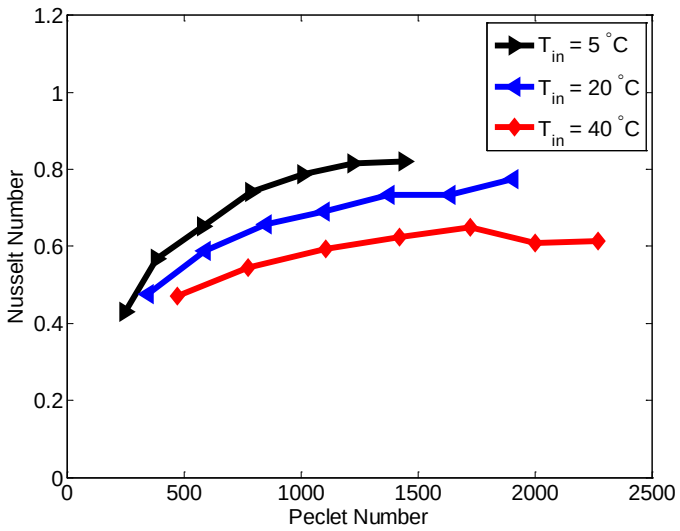

Figure 5: Nusselt number versus Peclet number

Figure 5 shows the measured Nusselt number as a function of the Peclet number. The data is plotted against the Peclet number because the Prandtl number of Tyfocor LS varies from about 100 at 5°C to 22 at 40°C. Laminar flow Nusselt numbers for channels with this aspect ratio will be expected lie between 1.148 and 6.29, depending on the boundary condition. However, the measured Nusselt numbers are much lower. Nusselt numbers of this order have been observed by several scholars who have experimentally and/or numerically studied heat transfer in micro-channels, for example, Dixit and Ghosh [21], Qu, et al. [22], Peng, et al. [18] and Wu and Cheng [50]. Various explanations have been postulated for these low Nusselt numbers. For example, Celata, et al. [47] attributed this to a heat loss term, Rahimi and Mehryar [32] and Nonino, et al. [51] attributed it to conjugate heat transfer (axial heat conduction in the duct wall). This paper investigates the effects of some of these phenomena

Figure 6 compares the measured and predicted friction factors; a similar trend can be observed in both predicted and measured values although measured friction factors are slightly lower than predicted values based on numerical Poiseuille numbers for rectangular channels (*Po*= 72.92 [52]). Lower friction factors in micro-channels have been observed in other studies, principally for gas flows [20, 53], but also for liquid flows [54, 55]. Deviation of friction factors from conventional theory is often attributed to surface roughness; however, surface roughness usually results in higher friction factors.

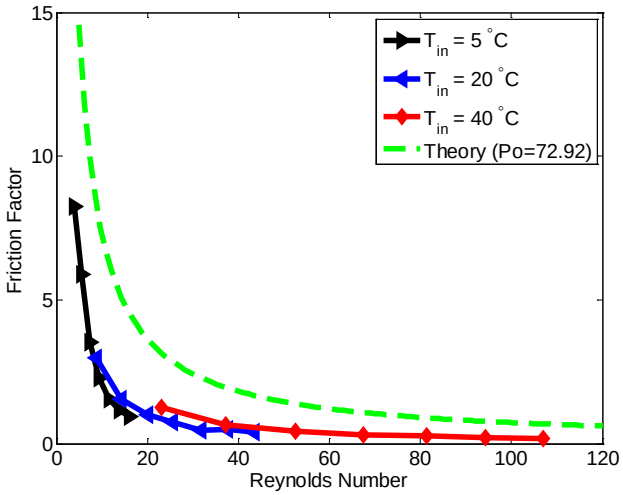

Figure 6: Friction factor versus Reynolds number

4.2 Viscous dissipation

A plot of Nusselt number against Brinkman number is shown in Figure 7. The curves can be seen to be almost horizontal lines with the exception of Nusselt numbers at lower Brinkman numbers (which correspond to lower flow velocities). At higher flow velocities viscous dissipation can result in lower Nusselt numbers [28, 30]. Figure 7 shows that the lower Nusselt numbers occur at lower Brinkman numbers (lower flow velocities) and are therefore not due to viscous dissipation. In addition, equation (2) yields *Br* less than equation (3) with ξ_{lim}=10%. The effects of viscous dissipation in the proposed design will therefore be insignificant at typical FPC operating conditions.

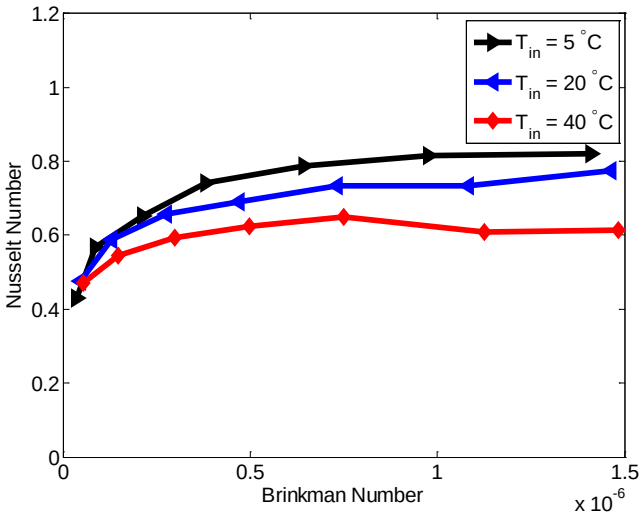

Figure 7: Brinkman number vs Nusselt number at various fluid temperatures

4.3 Entrance Effects

Figure 8 compares the local Nusselt number at different Graetz numbers. This Nusselt number is estimated by using the average heat flux, the measured plate temperature axially, *T(x)* and axial fluid temperature profile $T_f(x)$, from a model presented in Oyinlola, et al. [2], equation 25.

$$T_f(x) = \left[\frac{Sh}{\dot{m}c_p} \left(\frac{C_1}{\lambda_1} \left(e^{\lambda_1 x} - 1 \right) + \frac{C_2}{\lambda_2} \left(e^{\lambda_2 x} - 1 \right) \right) + \frac{Sq}{\dot{m}c_p} x \right]_0^X \tag{25}$$

A progressive decay of Nusselt number axially can be observed in Figure 8. A flow characterised by a significant developing entry region will yield a Nusselt number profile *Nu(x)* in the developing region and decay to a constant value in the fully developed region. The relationship between the percentage of flow in the thermally developing region and the Graetz number is shown in equation(26).

$$\frac{L_t}{L}(\%) = 5Gz \tag{26}$$

From this relationship, the percentage of thermally developing flow should be around 14%, 22.5% and 31.5% for *Gz* = 2.8, 4.5 and 6.3 respectively. This will imply that the local Nusselt number should be constant after these points. Also, since equation (5) is satisfied and *Gz*<10 the effects of entry length can be neglected [28, 30]. This signifies that the thermally developing region may not be the sole contributor to the observed profile.

The hydraulic entry length is difficult to measure experimentally; however, the thermal entry gives a good indication of the hydraulic entry length since $L_t = L_h Pr$. A computational fluid analysis may be an alternate method of measuring the hydraulic entry length in these micro-channels.

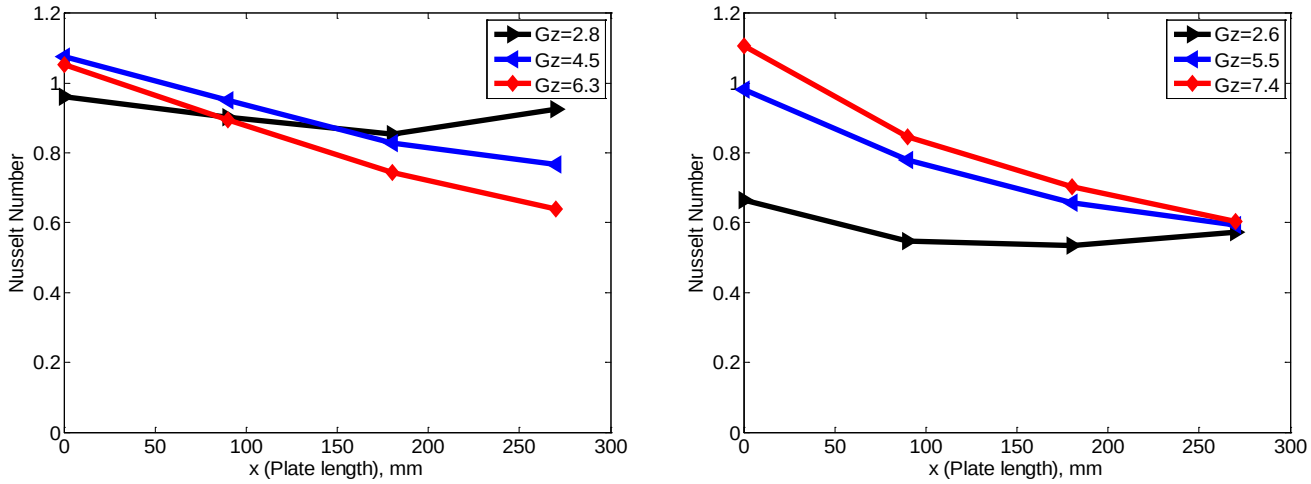

Figure 8: Local Nusselt number along the plate (a)T_{in} = 5°C (b) T_{in} = 20°C

Figure 9 shows the Nusselt numbers as a function of Graetz number. Nusselt number increases slightly and then becomes fairly constant. The heat transfer coefficient is enhanced in the thermal entry region; therefore, the Nusselt number is expected to be constant at low *Gz* numbers and then increase at high *Gz* when thermal entry length is significant. The profile observed supports the assumption that the entrance effects may not be the sole contributor to the profiles observed. If it was the sole contributor, a progressive increase of Nusselt number at higher *Gz* should be seen.

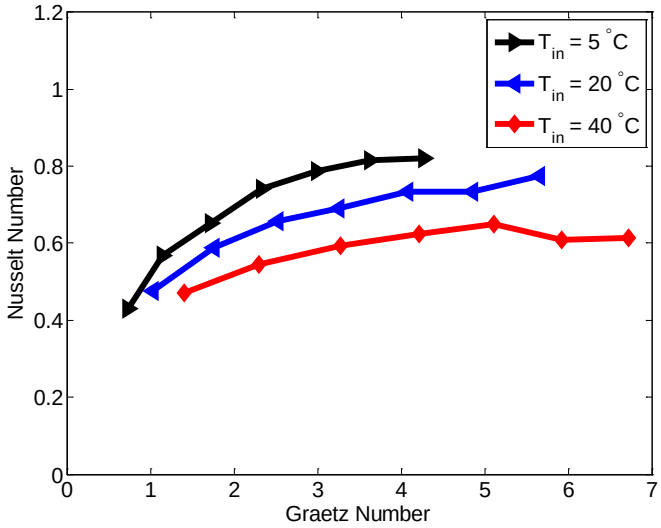

Figure 9: Nusselt number vs Graetz number at various fluid temperatures

4.4 Conjugate Heat Transfer

The thickness of the channel walls and the hydraulic diameter are similar hence thermal conduction in the walls can be significant. This might be responsible for the axial variation in local Nusselt number. The model presented by [2], shows that despite a uniform heat flux on the plate, axial thermal conduction can generate a plate temperature profile similar to an isothermal boundary at the entry and exit regions and a constant wall heat flux boundary in

between. Figure 10 compares profile of ΔT_{pf} from this model at two extreme cases. It can be seen that axial thermal conduction can yield significant axial variation in the plate temperature. This may further explain the axial variation of ΔT_{pf} observed in Figure 8 and Figure 9 above.

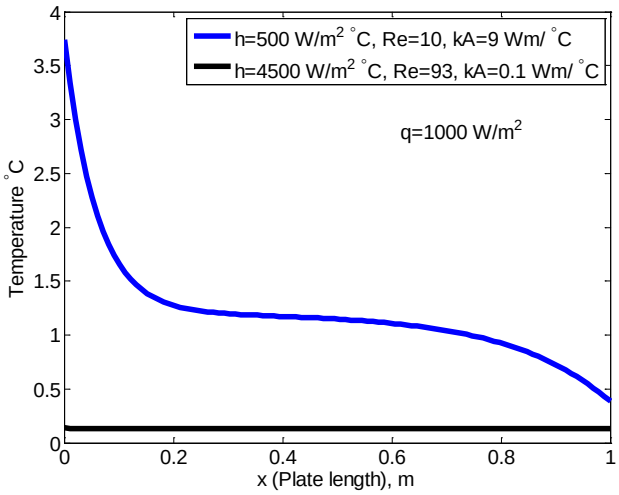

Figure 10: Profile of ΔT_{pf} at two extreme cases

Several Researchers have cited conjugate heat transfer as being responsible for lower Nusselt numbers [28, 30, 32, 51]. A plot of Nusselt number against axial conduction number is shown in Figure 11; an inverse relationship can be observed. This trend signifies that the axial conduction number has a negative impact on the Nusselt number which is in agreement with the proposition of Morini [28] and Rosa, et al. [30]. Since the axial conduction number was generally found to be greater than 0.01, satisfying equation (7), the effect of conjugate heat transfer is significant and should be accounted for in the proposed system. The axial variation of ΔT_{pf} can therefore be attributed to conjugate heat transfer. The significance of conjugate heat transfer may be lesser if the plates are manufactured differently, for example, hydro-formed channels will have a much lesser thickness than the current design.

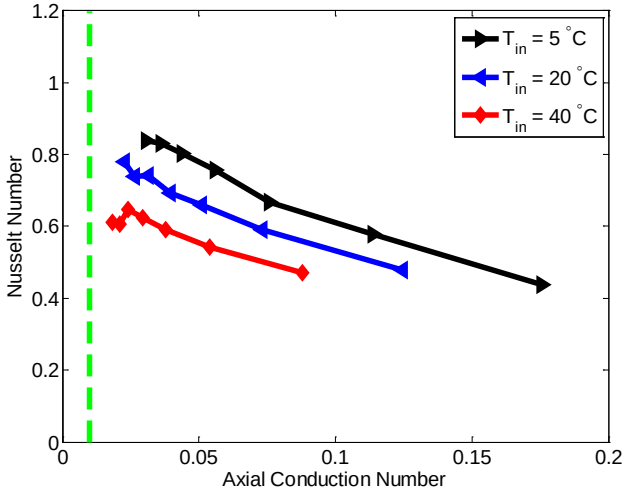

Figure 11: Nusselt number vs axial conduction number

4.5 Experimental Uncertainties

Another possible explanation for the discrepancies between experimental and theoretical results can be due to measurement uncertainties. Figure 12 shows a schematic of the experimental test rig used. The thermocouples measuring plate temperature were placed at the interface between top slab and micro-channel plate (with a fibre-glass adhesive layer between the top slab and the thermocouple tip). Thermocouples might have been reading a temperature at the interface rather than the plate temperature if there was significant thermal contact resistance between thermocouple tips and plate. Similarly, plate temperatures were read at 2 mm from the liquid/solid interface. Gamrat, et al. [23] observed that the position of the thermocouples away from the liquid/solid interface can yield as much as 40% uncertainty in the estimated Nusselt number. It should be noted that the accuracy of the measuring instruments as well as the repeatability of the experiment were validated. Therefore a correction can be applied to the temperature measurements using Fourier's law.

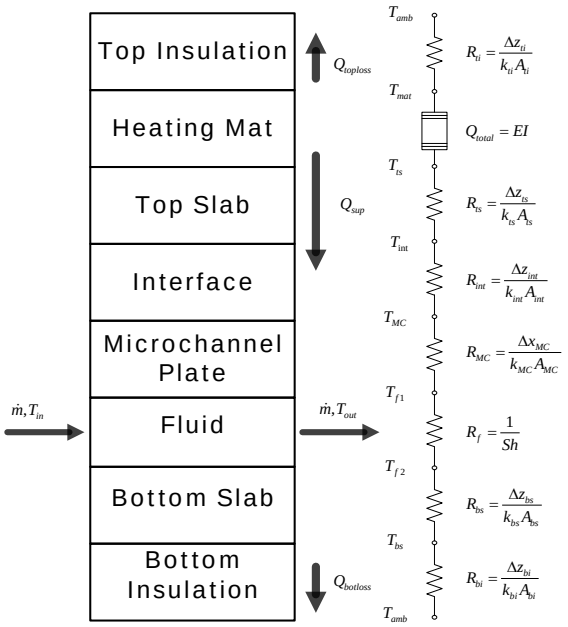

Figure 12: Schematic of thermal resistances in the test rig

The interface thickness was estimated by measuring the average thickness of the coupled test rig and subtracting it from the sum of the individual component thicknesses. This was found to be between 0.1 – 0.15 mm. This thickness was then used to estimate the temperature gradient across the interface and the plate temperature was corrected, assuming that measured temperature was in the middle of the interface.

$$T_{p,\text{corrected}} = T_p - \left(\frac{\Delta T_{\text{int}}}{2} + \Delta T_{\text{MCplate}} \right) \tag{27}$$

Where $\Delta T_{\text{MCplate}}$ is the temperature difference between the fluid solid interface and the top face of the micro-channel plate.

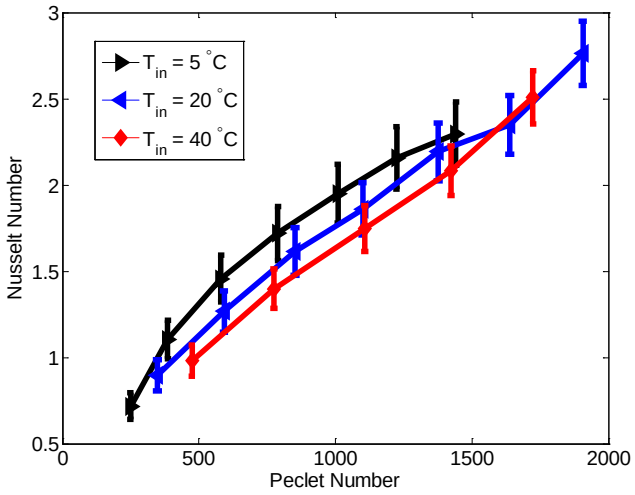

Figure 13: Corrected Nusselt numbers versus Peclet numbers

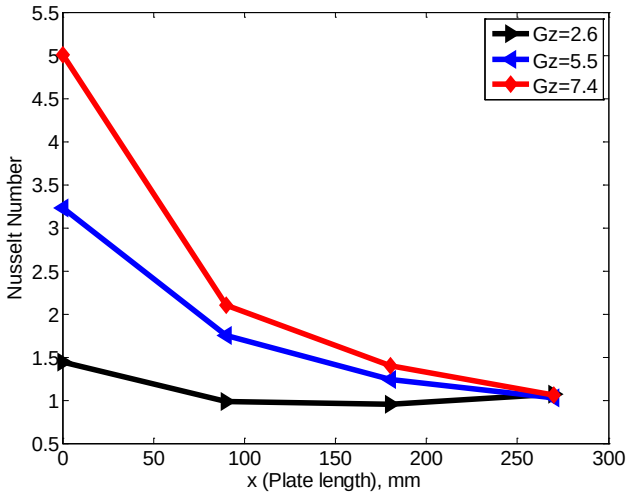

Figure 14: Corrected local Nusselt numbers

Figure 13, shows a plot of the corrected Nusselt numbers against Peclet numbers. The error bars in this figure account for other uncertainties such as fluid properties, flow rate and geometry. The corrected Nusselt numbers can be observed to be Peclet number dependent. This dependence can be attributed to the effect of axial conduction; from equation(23), the axial conduction number can be seen to be inversely proportional to the Peclet number. Figure 14 shows the corrected local Nusselt numbers; a similar trend to that observed in Figure 8b is seen here (i.e. Nusselt number decays axially), although the corrected Nusselt numbers are higher. Figure 15 shows the corrected average Nusselt number as a function of Axial Conduction number. A decay of the Nusselt number with axial conduction number can be observed; this agrees with the recommendation of Morini [28] and Rosa, et al. [30].

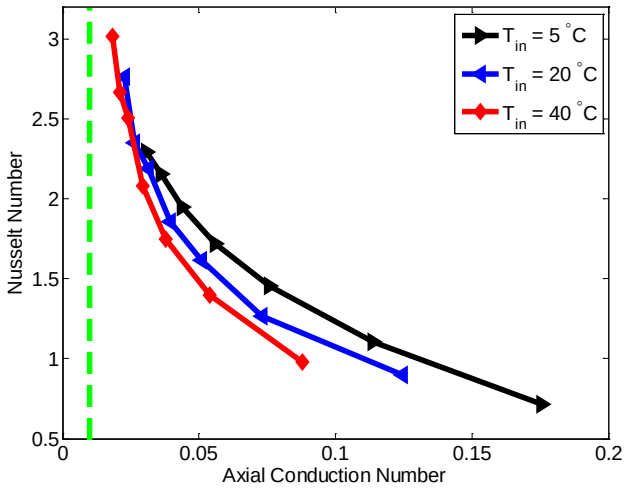

Figure 15: Corrected Nusselt number vs axial conduction number

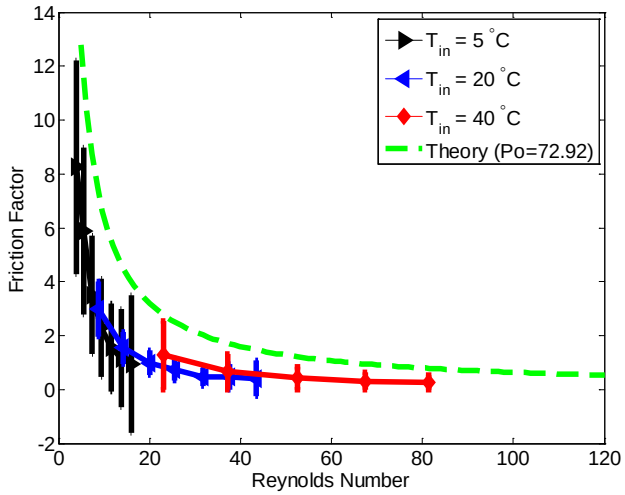

Figure 16: Friction factor versus Reynolds number

Figure 16 shows a plot of the corrected friction factor versus Reynolds number. The error bars in this figure account for uncertainties in fluid properties, geometry and measurements. It can be observed that the error bars are close to the theoretical values.

5. Conclusion

The significance of various scaling effects on the heat transfer and fluid flow in micro-channel absorber plates has been experimentally studied. Most of the scaling effects such as viscous dissipation and entrance effects were found to be insignificant. Nusselt number was found to reduce with the Axial conduction number, signifying that conjugate heat transfer has a negative impact on the Nusselt number, which agrees with previous studies. Thermal contact resistance between the top slab and micro-channel plate resulted in a significant thermal gradient at this interface which yielded lower calculated Nusselt numbers. Correcting the temperature measurements yielded Nusselt numbers that were close to conventional theory. Conjugate heat

transfer resulted in Peclet number dependent Nusselt number. Also, the corrected local Nusselt number was observed to vary axially despite satisfying the criteria for neglecting entrance effects; this variation increased with the Graetz number. The results are beneficial for the design and operation of micro-channel absorber plates.

Acknowledgments

This research used equipment through the Science City Energy project, part funded by the European Regional Development Fund, ERDF.

References

[1] UNEP. (2014). *.:: United Nations Environment Programme (UNEP) - SBCI*. Available: http://www.unep.org/sbci/AboutSBCI/Background.asp

[2] M. A. Oyinlola, G. S. F. Shire, and R. W. Moss, "Thermal analysis of a solar collector absorber plate with microchannels," *Experimental Thermal and Fluid Science,* 2014.

[3] G. P. Celata, "Heat transfer and fluid flow in microchannels," *Boiling and evaporation,* 2004.

[4] A. G. Hestnes, "Building Integration Of Solar Energy Systems," *Solar Energy,* vol. 67, pp. 181-187, 1999.

[5] Y. Tripanagnostopoulos, M. Souliotis, and T. Nousia, "Solar collectors with colored absorbers," *Solar Energy,* vol. 68, pp. 343-356, 2000.

[6] T. Matuska and B. Sourek, "Façade solar collectors," *Solar Energy,* vol. 80, pp. 1443-1452, 2006.

[7] P. B. L. Chaurasia, "Solar water heaters based on concrete collectors," *Energy,* vol. 25, pp. 703-716, 2000.

[8] B. Kundu, "Performance analysis and optimization of absorber plates of different geometry for a flat-plate solar collector: a comparative study," *Applied Thermal Engineering,* vol. 22, pp. 999-1012, 2002.

[9] V. Badescu, "Optimum fin geometry in flat plate solar collector systems," *Energy Conversion and Management,* vol. 47, pp. 2397-2413, 2006.

[10] S. Farahat, F. Sarhaddi, and H. Ajam, "Exergetic optimization of flat plate solar collectors," *Renewable Energy,* vol. 34, pp. 1169-1174, 2009.

[11] M. Rommel and W. Moock, "Collector efficiency factor F' for absorbers with rectangular fluid ducts contacting the entire surface," *Solar Energy,* vol. 60, pp. 199-207, 3// 1997.

[12] M. Khamis Mansour, "Thermal analysis of novel minichannel-based solar flat-plate collector," *Energy,* vol. 60, pp. 333-343, 2013.

[13] N. Sharma and G. Diaz, "Performance model of a novel evacuated-tube solar collector based on minichannels," *Solar Energy,* vol. 85, pp. 881-890, 2011.

[14] Y. Deng, Y. Zhao, W. Wang, Z. Quan, L. Wang, and D. Yu, "Experimental investigation of performance for the novel flat plate solar collector with micro-channel heat pipe array (MHPA-FPC)," *Applied Thermal Engineering,* vol. 54, pp. 440-449, 5/30/ 2013.

[15] R. K. Shah and A. L. London, *Laminar flow forced convection in ducts : a source book for compact heat exchanger analytical data*. New York: Academic Press, 1978.

[16] J. P. Holman, *Heat transfer*. Boston, [Mass.]: McGraw Hill Higher Education, 2010.

[17] D. B. Tuckerman and R. F. W. Pease, "High-performance heat sinking for VLSI," *IEEE Electron Device Lett. IEEE Electron Device Letters,* vol. 2, pp. 126-129, 1981.

[18] X. Peng, G. Peterson, and B. Wang, "Heat transfer characteristics of water flowing through microchannels," *Experimental Heat Transfer An International Journal,* vol. 7, pp. 265-283, 1994.
[19] X. F. Peng and G. P. Peterson, "Convective heat transfer and flow friction for water flow in microchannel structures," *International Journal of Heat and Mass Transfer,* vol. 39, pp. 2599-2608, 1996.
[20] S. B. Choi, R. R. Barren , and R. Q. Warrington, "Fluid flow and heat transfer in micro-tubes," *ASME DSC* pp. 89-93, 1991.
[21] T. Dixit and I. Ghosh, "Low Reynolds number thermo-hydraulic characterization of offset and diamond minichannel metal heat sinks," *Experimental Thermal and Fluid Science,* vol. 51, pp. 227-238, 11// 2013.
[22] W. Qu, G. M. Mala, and D. Li, "Heat transfer for water flow in trapezoidal silicon microchannels," *International Journal of Heat and Mass Transfer,* vol. 43, pp. 3925-3936, 11/1/ 2000.
[23] G. Gamrat, M. Favre-Marinet, and D. Asendrych, "Conduction and entrance effects on laminar liquid flow and heat transfer in rectangular microchannels," *International Journal of Heat and Mass Transfer,* vol. 48, pp. 2943-2954, 2005.
[24] T. M. Adams, S. I. Abdel-Khalik, S. M. Jeter, and Z. H. Qureshi, "An experimental investigation of single-phase forced convection in microchannels," *International Journal of Heat and Mass Transfer,* vol. 41, pp. 851-857, 1998.
[25] G. P. Celata, M. Cumo, M. Guglielmi, and G. Zummo, "Experimental investigation of hydraulic and single-phase heat transfer in 0.130-mm capillary tube," *Microscale Thermophysical Engineering,* vol. 6, pp. 85-97, 2002.
[26] A. Bucci, G. P. Celata, M. Cumo, E. Serra, and G. Zummo, "Water single-phase fluid flow and heat transfer in capillary tubes," in *ASME 2003 1st International Conference on Microchannels and Minichannels*, 2003, pp. 319-326.
[27] P.-S. Lee, S. V. Garimella, and D. Liu, "Investigation of heat transfer in rectangular microchannels," *International Journal of Heat and Mass Transfer,* vol. 48, pp. 1688-1704, 2005.
[28] G. L. Morini, "Scaling effects for liquid flows in microchannels," *Heat Transfer Engineering,* vol. 27, pp. 64-73, 2006.
[29] G. Hetsroni, A. Mosyak, E. Pogrebnyak, and L. P. Yarin, "Heat transfer in micro-channels: Comparison of experiments with theory and numerical results," *International Journal of Heat and Mass Transfer,* vol. 48, pp. 5580-5601, 2005.
[30] P. Rosa, T. Karayiannis, and M. Collins, "Single-phase heat transfer in microchannels: the importance of scaling effects," *Applied Thermal Engineering,* vol. 29, pp. 3447-3468, 2009.
[31] C. B. Sobhan and S. V. Garimella, "A comparative analysis of studies on heat transfer and fluid flow in microchannels," *Microscale Thermophysical Engineering,* vol. 5, pp. 293-311, 2001.
[32] M. Rahimi and R. Mehryar, "Numerical study of axial heat conduction effects on the local Nusselt number at the entrance and ending regions of a circular microchannel," *International Journal of Thermal Sciences,* vol. 59, pp. 87-94, 2012.
[33] G. Maranzana, I. Perry, and D. Maillet, "Mini-and micro-channels: influence of axial conduction in the walls," *International Journal of Heat and Mass Transfer,* vol. 47, pp. 3993-4004, 2004.
[34] V. V. Dharaiya and S. G. Kandlikar, "Numerical Investigation of Heat Transfer in Rectangular Microchannels Under H2 Boundary Condition During Developing and Fully

Developed Laminar Flow," *Journal of Heat Transfer,* vol. 134, pp. 020911-020911, 2011.
[35] G. L. Morini, "Viscous Dissipation as Scaling Effect for Liquid Flows in Microchannels (Keynote)," in *ASME 3rd International Conference on Microchannels and Minichannels*, 2005, pp. 93-102.
[36] M. G. Mala, D. Li, and J. D. Dale, "Heat transfer and fluid flow in microchannels," *International Journal of Heat and Mass Transfer,* vol. 40, pp. 3079-3088, 1997.
[37] G. L. Morini, "Single-phase convective heat transfer in microchannels: a review of experimental results," *International Journal of Thermal Sciences,* vol. 43, pp. 631-651, 2004.
[38] J. A. Duffie and W. A. Beckman, *Solar engineering of thermal processes*. Hoboken, N.J.: Wiley, 2006.
[39] J. Koo and C. Kleinstreuer, "Viscous dissipation effects in microtubes and microchannels," *International Journal of Heat and Mass Transfer,* vol. 47, pp. 3159-3169, 2004.
[40] G. Tunc and Y. Bayazitoglu, "Heat transfer in microtubes with viscous dissipation," *International Journal of Heat and Mass Transfer,* vol. 44, pp. 2395-2403, 2001.
[41] K. C. Toh, X. Y. Chen, and J. C. Chai, "Numerical computation of fluid flow and heat transfer in microchannels," *International Journal of Heat and Mass Transfer,* vol. 45, pp. 5133-5141, 2002.
[42] H. Herwig and S. P. Mahulikar, "Variable property effects in single-phase incompressible flows through microchannels," *International journal of thermal sciences,* vol. 45, pp. 977-981, 2006.
[43] H.-E. Jeong and J.-T. Jeong, "Extended Graetz problem including streamwise conduction and viscous dissipation in microchannel," *International Journal of Heat and Mass Transfer,* vol. 49, pp. 2151-2157, 2006.
[44] C.-H. Chen, "Slip-flow heat transfer in a microchannel with viscous dissipation," *Heat and mass transfer,* vol. 42, pp. 853-860, 2006.
[45] Z.-Y. Guo and Z.-X. Li, "Size effect on microscale single-phase flow and heat transfer," *International Journal of Heat and Mass Transfer,* vol. 46, pp. 149-159, 2003.
[46] P. Gao, S. Le Person, and M. Favre-Marinet, "Scale effects on hydrodynamics and heat transfer in two-dimensional mini and microchannels," *International Journal of Thermal Sciences,* vol. 41, pp. 1017-1027, 11// 2002.
[47] G. Celata, M. Cumo, V. Marconi, S. McPhail, and G. Zummo, "Microtube liquid single-phase heat transfer in laminar flow," *International Journal of Heat and Mass Transfer,* vol. 49, pp. 3538-3546, 2006.
[48] D. Tondeur, Y. Fan, J.-M. Commenge, and L. Luo, "Flow and pressure distribution in linear discrete “ladder-type” fluidic circuits: an analytical approach," *Chemical Engineering Science,* vol. 66, pp. 2568-2586, 2011.
[49] J. P. Holman, *Experimental methods for engineers*. Boston: McGraw-Hill/Connect Learn Succeed, 2012.
[50] H. Wu and P. Cheng, "An experimental study of convective heat transfer in silicon microchannels with different surface conditions," *International Journal of Heat and Mass Transfer,* vol. 46, pp. 2547-2556, 2003.
[51] C. Nonino, S. Savino, S. Del Giudice, and L. Mansutti, "Conjugate forced convection and heat conduction in circular microchannels," *International Journal of Heat and Fluid Flow,* vol. 30, pp. 823-830, 2009.

[52] Y. A. C. J. M. Çengel, *Fluid mechanics : fundamentals and applications*. Boston, Mass. [u.a.]: McGraw-Hill, 2010.
[53] J. C. Harley, Y. Huang, H. H. Bau, and J. N. Zemel, "Gas flow in micro-channels," *Journal of Fluid Mechanics,* vol. 284, pp. 257-274, 1995.
[54] B. Xu, K. Ooi, N. Wong, C. Liu, and W. Choi, "Liquid flow in microchannels," in *Proceedings of the 5th ASME/JSME Joint Thermal Engineering Conference*, 1999, pp. 1-7.
[55] J. Judy, D. Maynes, and B. Webb, "Liquid flow pressure drop in microtubes," in *International Conference on Heat Transfer and Transport Phenomena in Microscale, Banff, Canada*, 2000, pp. 149-154.